Octanuclear heterometallic Fe-III-Ce-IV pivalate clusters: From a close {Fe4Ce4(mu(4)-O)(4)} cage to an open {Fe4Ce4(mu(4)-O)(2)(mu(3)-O)(2)}

Inorganica Chimica Acta 515 (2021) 120038

Contents lists available at ScienceDirect

Inorganica Chimica Acta

journal homepage: www.elsevier.com/locate/ica

Research paper

Octanuclear heterometallic Fe^{III}-Ce^{IV} pivalate clusters: From a close $\{Fe_4Ce_4(\mu_4\text{-}O)_4\}$ cage to an open $\{Fe_4Ce_4(\mu_4\text{-}O)_2(\mu_3\text{-}O)_2\}$ core

Svetlana G. Baca[a,*], Francoise M. Amombo Noa[b], Lars Öhrström[b]

[a] Institute of Applied Physics, Academiei 5, 2028 Chisinau, Republic of Moldova
[b] Chemistry and Biochemistry, Department of Chemistry and Chemical Engineering, Chalmers University of Technology, SE 41296 Gothenburg, Sweden

ARTICLE INFO

Keywords:
Heterometallic 3d-4f compound
Octanuclear iron(III)-cerium(IV) cluster
Structure
Aminopolyalcohol ligand

ABSTRACT

Ultrasonic irradiation of trinuclear $[Fe_3O(O_2CCMe_3)_6(H_2O)_3]Me_3CCO_2{\cdot}2(Me_3CCO_2H)$ or hexanuclear $[Fe_6O_2(OH)_2(O_2CCMe_3)_{12}]$ pivalate precursors with $Ce(NO_3)_6{\cdot}6H_2O$, NaN_3 and triethanolamine (H_3tea) in MeOH/MeCN solution results in the synthesis of two new octanuclear Fe^{III}-Ce^{IV} clusters formulated as $[Fe_4Ce_4O_4(O_2CCMe_3)_4(tea)_4(N_3)_4(MeOH)_4]{\cdot}MeOH$ (**1**) and $[Fe_4Ce_4O_4(O_2CCMe_3)_6(tea)_4(N_3)_2(MeOH)_2]{\cdot}3(MeOH)$ (**2**). The spectroscopic and thermal properties of these compounds corroborate oxidation states and formula. Single crystal X-ray diffraction analysis revealed that the metal atoms in clusters **1** and **2** are organized in unprecedented close $\{Fe_4Ce_4(\mu_4\text{-}O)_4\}$ and open $\{Fe_4Ce_4(\mu_4\text{-}O)_2(\mu_3\text{-}O)_2\}$ cores, respectively. The topology of these cores has not been observed before in Fe^{III}-Ce^{IV} chemistry.

1. Introduction

Polynuclear cerium (IV)-oxo coordination compounds continue to attract attention because of their relation to the technologically important CeO_2 [1]. CeO_2 is classically used in self-cleaning ovens and catalytic converters for cars, but has emerging applications in catalysis for fuel cells, for the water–gas shift reaction, thermochemical water splitting, and organic reactions [2]. Cerium (III) and (IV) have also recently been incorporated into metal–organic frameworks [3], have been used for carbon dioxide reduction [4], and Ce^{IV} coordination chemistry has recently been reviewed [5].

Heterometallic 3d–4f discrete compounds have been in focus due to their potential in constructing single molecule magnets, SMMs [6]. In this respect Ce^{IV} might be thought less interesting as it has no unpaired electrons. However, with Mn^{III} polynuclear entities based on a $[Mn_8CeO_8]^{12+}$ core such materials have also been shown to generate SMM behaviour [7]. Mixed Ce–O–Fe compounds are, however, unusual, with just a handful well characterized, and this in recent years only [8–14]. Specifically, the combination of Ce^{IV} and Fe^{III} is uncommon, with a $[Fe^{III}_4Ce^{IV}_6O_8(L)_4(Me_3CCO_2)_{12}(RCO_2)_4]$ (HL = 3-amino-1-propanol or 2-(hydroxymethyl)piperidine; R = Me, C_2H_5, $ClCH_2$, $BrCH_2$) family reported by Kizas et al. [10] being the only structures closely related to the two compounds with an $\{Fe_4Ce_4O_4\}$ core that we will communicate here. Indeed, even $\{Ce_4O_4\}$ cores are unusual, there have been no examples of an isolated cube-based $\{Ce_4(\mu_3\text{-}O)_4\}$ cage reported, and the open $\{Ce_4(\mu_3\text{-}O)_2(\mu_2\text{-}O)_2\}$ motif, while being present in some 60 structures in the Cambridge Structural Database (CSD), there are only a few containing Ce^{IV}, including two MOFs [15,16].

It is necessary to note that for the preparation of polynuclear heterometallic 3d-4f coordination clusters, the use of multiple organic ligands having N- and O-donor sites such as amino alcohols and carboxylic acids, which display both chelating and bridging coordination modes and capable simultaneously bind 3d and 4f metal atoms, was the most successful strategy in many cases [see for example 6,17,18]. We also explored the advantages of using both structure-directing amino alcohols and carboxylate bridges for the creation of heterometallic coordination cluster families [19–25].

It is important to note that these synthetic procedures are multi-component reactions where a previously isolated polynuclear entity is reacted with at least two new ligands and another metal ion. Given the multitude of products conceivable from such mixtures, the control and development of these reactions to give high yield and high purity products is a major undertaking, and vital for the development of inorganic synthesis.

In this case our synthetic methodology has been adopted to develop a straightforward protocol to heterometallic Fe-Ce containing clusters, using μ_3-oxo trinuclear or hexanuclear Fe^{III} pivalate precursors and tetratopic triethanolamine (H_3tea) and azide ligands, both having the ability to bridge different types of metal ions (Scheme 1). Moreover, the source of cerium cations in the synthetic procedure was $Ce(NO_3)_6{\cdot}6H_2O$ with presumably the more stable oxidation state +3 for Ce, which under synthetic conditions were oxidized to Ce^{IV}. The approach

* Corresponding author.
E-mail address: sbaca_md@yahoo.com (S.G. Baca).

https://doi.org/10.1016/j.ica.2020.120038
Received 6 August 2020; Received in revised form 21 September 2020; Accepted 21 September 2020
Available online 24 September 2020

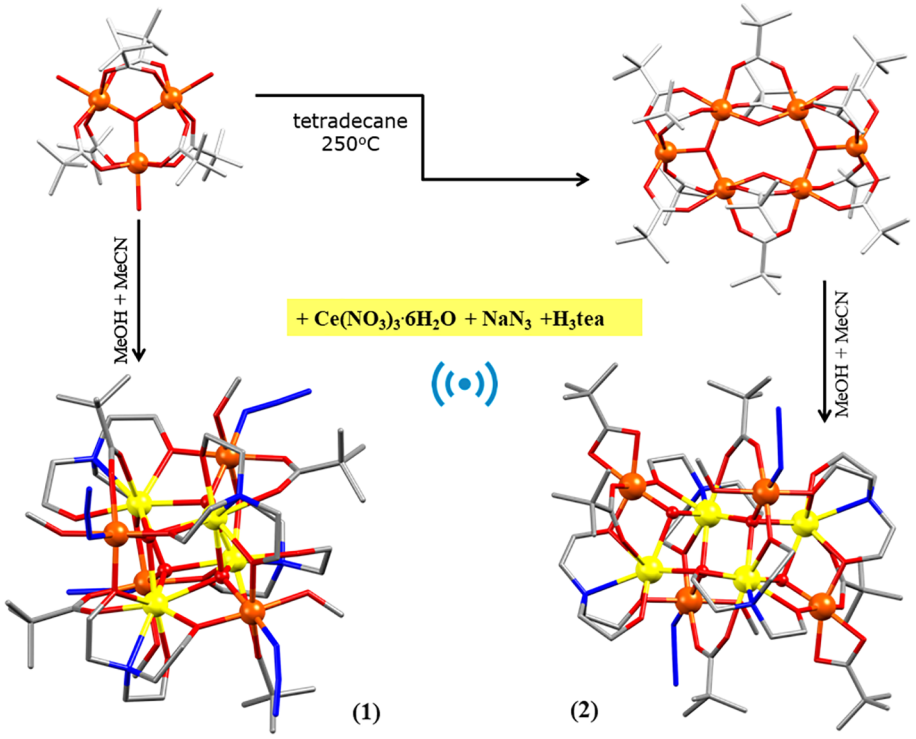

Scheme 1. Synthesis of $[Fe_4Ce_4O_4(O_2CCMe_3)_4(tea)_4(N_3)_4(MeOH)_4]\cdot MeOH$ (**1**) and $[Fe_4Ce_4O_4(O_2CCMe_3)_6(tea)_4(N_3)_2(MeOH)_2]\cdot 3(MeOH)$ (**2**). Fe: orange, Ce: yellow spheres; O: red, C: light grey, N: blue sticks. Oxo-ligands are highlighted as red balls. Hydrogen atoms and solvent molecules are omitted for clarity. The "sound symbol" indicates ultrasonic irradiation.

mentioned above resulted in remarkable octanuclear Fe^{III}-Ce^{IV} coordination clusters, namely $[Fe_4Ce_4O_4(O_2CCMe_3)_4(tea)_4(N_3)_4(MeOH)_4]\cdot MeOH$ (**1**) and $[Fe_4Ce_4O_4(O_2CCMe_3)_6(tea)_4(N_3)_2(MeOH)_2]\cdot 3(MeOH)$ (**2**), with unprecedented close $\{Fe_4Ce_4(\mu_4\text{-}O)\}$ and open $\{Fe_4Ce_4(\mu_4\text{-}O)_2(\mu_3\text{-}O)_2\}$ cores. The synthesis and structural features of these clusters will be discussed here in detail.

2. Experimental section

2.1. Materials and physical measurements

All reagents were purchased from commercial sources and used without further purification. All reactions were carried out under aerobic conditions using commercial grade solvents. $[Fe_3O(O_2CCMe_3)_6(H_2O)_3]Me_3CCO_2{\cdot}2(Me_3CCO_2H)$ and $[Fe_6O_2(OH)_2(O_2CCMe_3)_{12}]$ were synthesized as described elsewhere [26,27]. *Caution! Care should be taken when using the potentially explosive sodium azide.* The infrared spectra were recorded on a Perkin-Elmer Spectrum Series 815 FT-IR spectrometer in the region 4000–400 cm^{-1}. The UV–Vis absorption spectra were measured with a PerkinElmer Lambda 900 UV–Vis-NIR Spectrometer. TGA measurements were carried out with a Mettler Toledo TGA/DSC 3^+ in air at a heating rate of 10 K min^{-1} from 30 °C to 800 °C. Ultrasonic irradiation was executed in an ultrasonic cleaner Elmasonic P at the frequency of 37 kHz.

2.2. Single crystal X-ray crystallography

Single crystal data for **1** was collected at 297(2) K using a Bruker APEX DUO diffractometer with MoKα, radiation (λ = 0.71073 Å). Data reduction was conducted using the SAINT-Plus software [28], while the absorption corrections were performed using the SADABS program [29,30]. For **2**, X-ray measurements were performed at 100.01(16) K with a Rigaku Synergy, Dualflex, AtlasS2 diffractometer using CuKα radiation (λ = 1.54184 Å) and the CrysAlis PRO 1.171.38.43 suite. In structure **2**, CCD data were extracted and integrated using CrysAlis [31,32]. Direct methods were used for all structures and the refinements were established by full-matrix least squares with SHEL-2018/3 [33] using the X-seed platform [34]. All non-hydrogen atoms in both structures were found in the difference electron map and refined anisotropically except in the case of disordered molecules. All hydrogens except the hydroxyl hydrogens were placed with geometric constraints and refined isotropically. The crystallographic data and structure refinement parameters for **1** and **2** are listed in Table 1. The selected bond distances for **1** and **2** are given in Table 2 and additional crystallographic information about angles in coordination polyhedra and hydrogen bond interactions is available in the Supporting Information, Tables S1 and S2. Packing diagrams for compounds **1** and **2** are shown

Table 1
Crystallographic data and structure refinement parameters for **1** and **2**.

Code	1	2
Structural formula	$C_{49}H_{104}Ce_4Fe_4N_{16}O_{29}$	$C_{59}H_{122}Ce_4Fe_4N_{10}O_{33}$
Molecular mass (g mol^{-1})	2165.36	2283.54
Data collection temp. (K)	297(2)	100(2)
Crystal system	Monoclinic	Triclinic
Space group	C_2	$P\bar{1}$
a (Å)	26.2664(12)	12.2059(2)
b (Å)	12.1527(6)	13.3098(2)
c (Å)	14.2140(7)	15.9344(2)
α (°)	90	110.730(1)
β (°)	114.8500(10)	98.525(1)
γ (°)	90	110.735(1)
Volume ($Å^3$)	4117.1(3)	2150.71(4)
Z	2	1
D_c, calc density (g cm^{-3})	1.747	1.763
Absorption coefficient (mm^{-1})	2.927	21.944
θ range	2.677–26.435	3.12–67.06
Reflections collected	20,302	21,958
Independent reflections	8397 [R_{int} = 0.0297]	7567 [R_{int} = 0.0373]
Data / restraints / parameters	8397 / 4 / 477	
Final R indices [$I > 2$ sigma (I)]	R_1 = 0.0292 wR_2 = 0.0609	R_1 = 0.0305 wR_2 = 0.0812
R indices (all data)	R_1 = 0.0367 wR_2 = 0.0632	R_1 = 0.0331 wR_2 = 0.0827
Goodness-of-fit on F^2	1.022	1.046
Largest diff. peak and hole ($e{\cdot}Å^{-3}$)	0.548 and − 0.387	1.205 and − 0.937
CCDC no.	2019599	2019600

Table 2
Selected bond distances (Å) for **1** and **2**.

1			
Ce1–O9	2.179(5)	Ce2–O2	2.445(4)
Ce1–O2	2.294(4)	Ce2–N2	2.651(6)
Ce1–O8	2.301(5)	Fe1–O7	1.980(5)
Ce1–O7	2.314(5)	Fe1–O8$^{\#1}$	1.982(5)
Ce1–O1$^{\#1}$	2.365(4)	Fe1–N3	1.990(7)
Ce1–O5	2.397(5)	Fe1–O1	1.996(5)
Ce1–O1	2.437(4)	Fe1–O3	2.035(5)
Ce1–N1	2.665(6)	Fe1–O13	2.095(5)
Ce2–O11	2.193(5)	Fe2–O10	1.976(5)
Ce2–O1$^{\#1}$	2.296(4)	Fe2–O12$^{\#1}$	1.984(5)
Ce2–O12	2.306(5)	Fe2–O2	1.992(4)
Ce2–O10	2.315(5)	Fe2–N6	2.015(6)
Ce2–O2$^{\#1}$	2.369(4)	Fe2–O6	2.052(5)
Ce2–O4$^{\#1}$	2.376(5)	Fe2–O14	2.110(5)
Metal…Metal			
Ce1–Fe1$^{\#1}$	3.4406(11)	Ce2–Fe2$^{\#1}$	3.4473(11)
Ce1–Fe1	3.4886(11)	Ce2–Fe2	3.4992(11)
Ce1–Ce1$^{\#1}$	3.7578(7)	Ce2–Ce2$^{\#1}$	3.7641(8)
Ce1–Ce2	3.7683(5)		
#1–x + 1, y , −z + 1			
2			
Ce1–O10	2.118(3)	Ce2–O8	2.390(3)
Ce1–O9	2.327(3)	Ce2 − N2	2.648(3)
Ce1–O13$^{\#1}$	2.355(3)	Fe1–O9	1.974(3)
Ce1–O3	2.378(3)	Fe1–O14	1.983(3)
Ce1–O2	2.384(3)	Fe1–N3	2.009(3)
Ce1–O1	2.385(3)	Fe1–O1	2.012(2)
Ce1–O11	2.394(3)	Fe1–O7$^{\#1}$	2.034(3)
Ce1–N1	2.668(3)	Fe1–O15	2.105(3)
Ce2–O2	2.273(3)	Fe2–O2	1.912(3)
Ce2–O13	2.286(3)	Fe2–O11	1.947(3)
Ce2–O1$^{\#1}$	2.312(2)	Fe2–O12	1.991(3)
Ce2–O14	2.345(3)	Fe2–O4	2.079(3)
Ce2–O12	2.352(3)	Fe2–O6	2.098(3)
Ce2–O1	2.378(2)	Fe2–O5	2.115(3)
Metal…Metal			
Ce1–Fe2	3.3605(6)	Ce1–Ce2	3.7518(3)
Ce1–Fe1	3.4159(6)	Ce1–Ce2$^{\#1}$	3.7815(3)
Ce2–Fe2	3.3830(6)	Ce2–Ce2$^{\#1}$	3.7636(4)
Ce2–Fe1	3.4937(6)		
#1 − x + 1, −y, −z			

in Figs. S3 and S4, Supporting Information. The DIAMOND [Diamond Version 3.2 h 1997–2012 Crystal Impact GbR, Bonn, Germany] software suite and Mercury SCD 4.3.0 program were used for graphical representation.

2.3. Syntheses of $[Fe_4Ce_4O_4(O_2CCMe_3)_4(tea)_4(N_3)_4(MeOH)_4]\cdot MeOH$ (1) and $[Fe_4Ce_4O_4(O_2CCMe_3)_6(tea)_4(N_3)_2(MeOH)_2]\cdot 3(MeOH)$ (2)

$[Fe_4Ce_4O_4(O_2CCMe_3)_4(tea)_4(N_3)_4(MeOH)_4]\cdot MeOH$ (1): To the solution of $[Fe_3O(O_2CCMe_3)_6(H_2O)_3]O_2CCMe_3\cdot 2(Me_3CCO_2H)$ (0.115 g, 0.1 mmol), $Ce(NO_3)_3\cdot 6H_2O$ (0.130 g, 0.3 mmol), and sodium azide (0.02 g, 0.3 mmol) in MeCN (6 mL) was added a solution of triethanolamine (0.37 g, 2.5 mmol) in MeOH (6 mL). The resulting solution was treated under ultrasonic irradiation for 30 min and then filtered. The filtrate was left for slowly evaporation of the mother solution at room temperature. This gave orange crystals suitable for X-ray analysis after two weeks. The crystals of **1** were filtered off, washed with MeCN and dried in air. Yield: 0.082 g (52% based on Fe). TGA is consistent with the compound as formulated. IR (cm^{-1}): 3450 (br.w), 2956 (w), 2859 (m), 2062 (s), 1530 (s), 1482 (m), 1460 (m), 1442 (m), 1417 (s), 1374 (m), 1359 (s), 1338 (sh), 1226 (m), 1085 (sh), 1070 (vs), 1062 (vs), 1031 (sh), 1015 (sh), 925 (m), 903 (vs), 878 (sh), 810 (w), 784 (w), 748 (w), 617 (sh), 601 (sh), 582 (sh), 570 (s), 526 (m), 491 (vs).

$[Fe_4Ce_4O_4(O_2CCMe_3)_6(tea)_4(N_3)_2(MeOH)_2]\cdot 3(MeOH)$ (2): To the solution of $[Fe_6O_2(OH)_2(O_2CCMe_3)_{12}]$ (0.04 g, 0.025 mmol), $Ce(NO_3)_3\cdot 6H_2O$ (0.07 g, 0.16 mmol), and sodium azide (0.02 g, 0.3 mmol) in MeCN (6 mL) was added a solution of triethanolamine (0.37 g, 2.5 mmol) in MeOH (6 mL). The resulting solution was treated under ultrasonic irradiation for 30 min and then filtered. The filtrate was left for slow evaporation of the mother solution at room temperature. The orange crystals of **2** suitable for X-ray analysis were filtered off after one month, washed with MeCN and dried in air. Yield: 0.052 g (62% based on Fe). TGA is consistent with the compound as formulated. IR (cm^{-1}): 3450 (br.w), 3150 (br.w), 2957 (w), 2846 (m), 2061 (s), 1534 (s), 1480 (m), 1458 (m), 1410 (m), 1357 (s), 1343 (s), 1219 (m), 1074 (vs), 1035 (sh), 1018 (sh), 991 (sh), 915 (sh), 903 (s), 786 (w), 747 (w), 628(sh), 603(sh), 579 (s), 550 (s), 521 (s), 472 (s).

3. Results and discussion

3.1. Synthesis and preliminary characterization

The heterometallic octanuclear clusters $[Fe_4Ce_4O_4(O_2CCMe_3)_4(tea)_4(N_3)_4(MeOH)_4]\cdot MeOH$ (**1**) and $[Fe_4Ce_4O_4(O_2CCMe_3)_6(tea)_4(N_3)_2(MeOH)_2]\cdot 3(MeOH)$ (**2**) have been prepared, as shown in Scheme 1, starting from the well-known μ_3-oxo trinuclear pivalate precursor $[Fe_3O(O_2CCMe_3)_6(H_2O)_3]O_2CCMe_3\cdot 2(Me_3CCO_2H)$ [26]. This trinuclear pivalate complex has been previously used as a starting material in the synthesis of a wide range of homometallic polynuclear cluster compounds like $\{Fe_8\}$, [35], $\{Fe_{11}\}$ [36], $\{Fe_{14}\}$ [37], and $\{Fe_{16}\}$ [36], as well as a series of heterometallic Fe-Ln clusters [19,24]. The ultrasonic treatment of the trinuclear pivalate precursor with cerium(III) nitrate hexahydrate, sodium azide and triethanolamine in a methanol/acetonitrile solution for 30 min results in the heterometallic octanuclear cluster **1** in ca. 50% yield. Interesting, the cerium ions in **1** form a central cube-like $\{Ce_4(\mu_3\text{-}O)_4\}$ core surrounding by four Fe(III) ions.

In the other reaction, heating of the μ_3-oxo trinuclear pivalate in tetradecane leds to a hexanuclear pivalate cluster $[Fe_6O_2(OH)_2(O_2CCMe_3)_{12}]$ [27]. Using hexanuclear pivalates instead of trinuclear precursors under the same reaction conditions afforded the heterometallic octanuclear cluster **2** in ca. 60% yield. In contrast to **1**, the core of cluster **2** consists of an open $\{Ce_4(\mu_3\text{-}O)_2(\mu_2\text{-}O)_2\}$ unit that is encircled by four Fe(III) ions.

The infrared spectra of **1** and **2** display strong and broad bands in the region of 1534–1530 and 1417–1410 cm^{-1}, arising from asymmetric and symmetric stretching vibrations of the coordinated carboxylate groups of the pivalate ligands, respectively. The C—H asymmetric and symmetric stretch vibrations for tert-butyl groups of pivalates and $-CH_2-$ groups of tea^{3-} are observed in the 2957 – 2846 cm^{-1} region, along with peaks at 1482–1480 cm^{-1} and 1359–1343 cm^{-1}, which correspond to asymmetric and symmetric bending vibrations for methyl and methylene groups, respectively. The presence of the hydroxyl groups of MeOH caused the appearance of broad absorption bands in the region of 3450–3150 cm^{-1}. A very strong peak in each spectrum at 2062–2061 cm^{-1} corresponds to the N≡N stretching vibrations of the azide ligands.

Thermogravimetric analysis (TGA) of **1** and **2** (Figs. S5 and S6) showed that both compounds exhibit similar thermal behavior and at the beginning of heating they release the coordinated and solvent methanol molecules. Cluster **1** loses five methanol molecules before 215 °C (observed 6.6%, calculated 7.4%) and then, on further heating, the azide and the remaining organic parts decompose in several weakly resolved steps correlating exactly with its differential scanning calorimetry (DSC). The remaining mass at 800 °C, 43.5%, corresponds well to the calculated 46.6%. The thermal analysis of **2** was more complex than **1** due to further steps. For **2**, a first weight loss of 4.4% corresponds to the release of solvent methanol molecules (calculated 4.2%) before 190 °C. The second weight loss of 3.3% (calculated 2.8%) may be attributed to the methanol ligands at 220 °C. Before 315 °C there is a mass loss of 28.3% which may be decomposition of the remaining ligands except the carboxylates (calculated at 29.3%). On further heating, the carboxylate decompose. On the DSC trace it looks like the last step is also accompanied by a recrystallisation. The remaining mass at 800 °C, 45.8%, corresponds well to the calculated 44.1%.

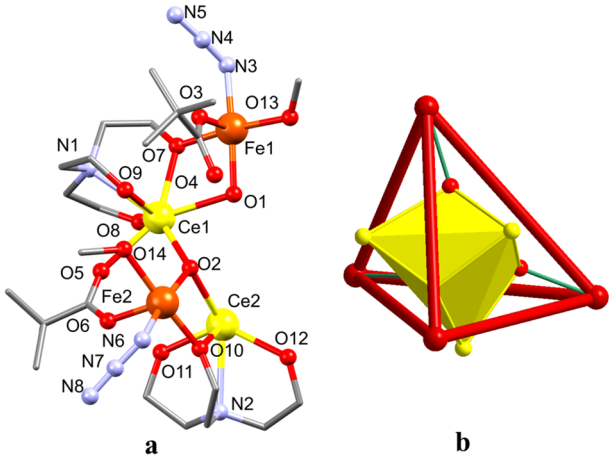

Fig. 1. Asymmetric unit in **1** with a partial numbering (a). View of the arrangement of metal atoms as "cube in tetrahedron" in **1** (b). Fe: orange, Ce: yellow spheres; O: red, N: blue ball; C: light grey sticks. Hydrogen atoms and solvent molecules are omitted for clarity. (For interpretation of the references to colour in this figure legend, the reader is referred to the web version of this article.)

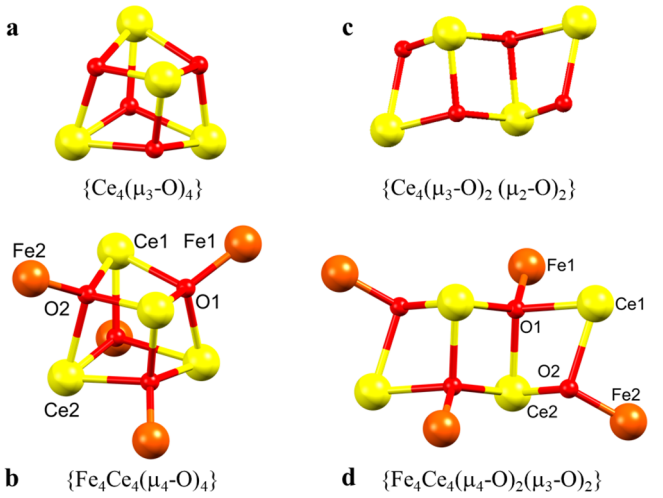

Fig. 2. View of a close cubane-like $\{Fe_4Ce_4(\mu_4\text{-}O)_4\}$ core (a, b) and an open $\{Fe_4Ce_4(\mu_4\text{-}O)_2(\mu_3\text{-}O)_2\}$ core (c, d) in **1** and **2**, respectively.

3.2. Crystal structure analysis

Single-crystal X-ray diffraction analysis showed that compound **1** crystallizes in the monoclinic space group C_2 and the asymmetric unit contains half of the cluster (two iron atoms, two cerium atoms, two oxo anions, two pivalate groups, two fully deprotonated amino-alcohol ligands, two azide anions, and two methanol molecules) and one disordered methanol molecule (Fig. 1a). Charge consideration of **1** and BVS (bond valence scheme [38–40]) calculations indicate that Fe centers are in the 3+ oxidation state (Fe1, Fe2, BVS – 3.07 and 3.01), whereas Ce centers are in the 4+ oxidation state (Ce1, Ce2, BVS – 4.03 and 3.99). Thus, the cluster core of **1** is composed of four Fe^{III} and four Ce^{IV} ions bridged by four μ_4-oxo groups, four bridging pivalate residues and additionally linked by four fully deprotonated tea^{3-} ligands. Azide N_3^- anion and neutral MeOH additionally cup each of the Fe^{III} centers thus completing the coordination sphere of the ions. This results in an octahedral surrounding for all iron atoms with a NO_5 donor set by a μ_4-oxo atom, one O atom from bridging pivalate, three O atoms from different tea^{3-} ligands and a N atom from azide.

The Fe^{III}–O bond distances are in the range of 1.976(5) – 2.110(5) Å and the Fe^{III} – N bond distances equal to 1.990(7) and 2.015(6) Å (Table 2). All Ce atoms have a dodecahedral NO_7 geometry by three μ_4-oxo atoms, an O atom from a bridging carboxylate, three O and one N atoms from tea^{3-} ligand. The Ce^{IV}–O bond distances range from 2.179(5) to 2.445(4) Å and Ce^{IV}–N bond distances are 2.651(6) and 2.665(6) Å (Table 2). The Fe^{III}–O and Ce^{IV}–O bond distances in **1** are similar to other reported Fe^{III} and Ce^{IV} compounds as evident from comparison of the formal oxidation state in the majority of homometallic six-coordinated Fe^{II}/Fe^{III}–O and eight-coordinated Ce^{III}/Ce^{IV}–O analogues complexes stored in the Cambridge Structural Database (CSD) (Figs. S1 and S2, Supplementary Information). Additionally, the oxidation state of Ce atoms was supported by UV–vis spectroscopic data that revealed variable ligand-to-metal charge transitions [41] (Figs. S7 and S8, Supplementary Information).

The heterometallic octanuclear cluster **1** can also be viewed as a central cubane-like $\{Ce_4(\mu_3\text{-}O)_4\}$ subunit surrounded by four Fe^{III} atoms which form a tetrahedron as shown in Fig. 1b and 2a,b. The cuboidal core is distorted with all Ce–(μ_3-O)–Ce angles in the range of 102.87(2) – 108.21(2)° and (μ_3-O)–Ce–(μ_3-O) of 70.30(2) – 73.42(2)° (Table S1, Supplementary Information). The metal–metal separations in the cube are close within the range of 3.758(8)–3.768(5) Å. As mentioned above, this kind of structural topology is quite rare in the 3d/4f complexes with no reports for a Ce-containing family. The tetrahedron defined by the Fe sites is irregular with all triangular faces being isosceles (two longer Fe···Fe separations of 6.219(2) and 6.233(1) Å and one short Fe···Fe separation of 5.361(1) Å) (Fig. 1b). The crystal packing of **1** is shown in Fig. S3 (Supplementary Information). There are strong intramolecular O—H···O hydrogen bonding interactions of 2.578(8) and 2.580(7) Å between oxygen atoms (O13, O14) of the coordinated methanol molecules and oxygen atoms of tea^{3-} ligands (O11, O9) (Table S2, Supplementary Information).

Single-crystal X-ray diffraction analysis showed that compound **2** crystallizes in the triclinic space group *P*-1 and the asymmetric unit contains two iron atoms, two cerium atoms, two oxo anions, three pivalate groups, two fully deprotonated amino alcohol ligands, an azide anion, a methanol molecule, and one and half solvent methanol molecules (Fig. 3a). Similar to **1**, oxidation states for metal atoms have been assigned on the basis of bond valence sum analysis (BVS [38–40]), and by consideration of bond distances (Figs. S1, S2) and charge balance: Fe centers are in the 3+ oxidation state (Fe1 and Fe2, BVS – 3.02 and 2.94), and Ce centers are in the 4+ oxidation state (Ce1 and Ce2, BVS – 3.99 and 3.90).

Additionally, the oxidation state of Ce atoms in **2** was supported by its electronic absorption spectra that show broad features corresponding to variable LMCT → 5d Ce^{IV} and LMCT → 4f Ce^{IV} transitions [41] (Figs. S7 and S8, Supplementary Information). Thus, the cluster core of **2** is composed of four Fe^{III} and four Ce^{IV} ions bridged by two μ_3-oxo and two μ_4-oxo groups forming a $\{Fe_4Ce_4(\mu_4\text{-}O)_2(\mu_3\text{-}O)_2\}$ core (Fig. 2c,d), and additionally linked by four bridging pivalate residues and four fully deprotonated tea^{3-} ligands. Azide N_3^- anion and neutral MeOH additionally complete the coordination sphere of the Fe1 (and its symmetry partner) atoms, whereas the chelating pivalate cups Fe2 (and its symmetry partners) atoms.

In cluster **2**, Fe^{III} ions are six–coordinated and adopt distorted octahedral geometries. Fe1 (and its symmetry partner) have an NO_5 donor set by a μ_4-oxo, an oxygen carboxylate atom from bridging pivalate, two oxygen atoms from fully deprotonated tea^{3-} ligands and an oxygen atom from the coordinated methanol molecule [Fe1–O bond distances range from 1.974(3) to 2.105(3) Å], and a N atom of an azide ion [Fe1–N, 2.009(3) Å]. Fe2 (and its symmetry partner) have an O_6 environment by a μ_3-oxo atom, three O atoms from chelating and bridging pivalates and two O atom of two different tea^{3-} ligands with Fe^{III}–O distances in the range of 1.912(3) – 2.115(3) Å (Table 2). All Ce^{IV} atoms are eight-coordinated having the distorted dodecahedral NO_7 geometries. The coordination environment of Ce1 (and its symmetry partner) atom with Ce–O bond distances of 2.118(3) – 2.394(3) Å and Ce–N bond distance equals to 2.668(3) Å is completed through μ_3-O and μ_4-O groups, four O atoms and one N atom coming from two tea^{3-} ligands, and an O atom of bridging pivalate, whereas Ce2 (and its symmetry partner) atom is surrounded by two μ_3-O and one μ_4-O groups, three O

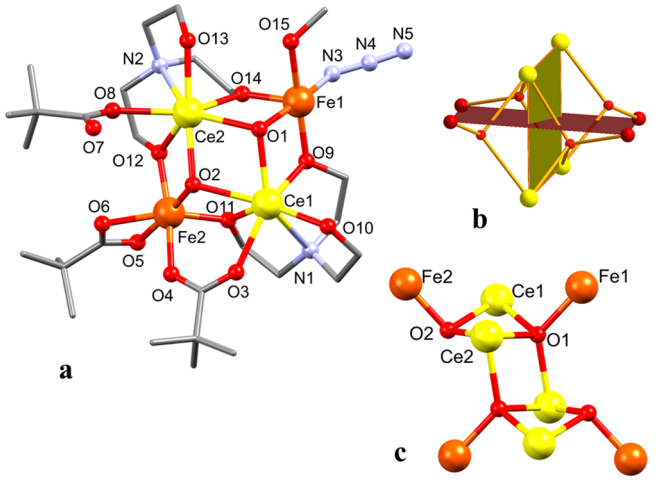

Fig. 3. Asymmetric unit in **2** with a partial numbering (a). Octanuclear core of cluster **2** showing the coplanar arrangement of Ce^{IV} ions (shaded green) and Fe^{III} ions (shaded burgundy) (b). The $\{Fe_4Ce_4(\mu_4\text{-}O)_2(\mu_3\text{-}O)_2\}$ core of **2** emphasizing the joined butterfly-like subunits (c). Fe: orange, Ce: yellow spheres; O: red, N: blue ball; C: light grey sticks. Hydrogen atoms and solvent molecules are omitted for clarity. (For interpretation of the references to colour in this figure legend, the reader is referred to the web version of this article.)

atoms and one N atom from one tea^{3-} ligand, and an O atom of bridging pivalate [Ce–O, 2.273(3) – 2.390(3) Å; Ce–N, 2.648(3) Å]. The Ce/Fe–O/N bond distances are comparable to the corresponding value found in **1** and in previously reported Fe-Ce clusters [10].

The core structure of compound **2** has a central tetranuclear arrangement of four Ce^{IV} ions (Ce1, Ce2 and their symmetry partners) flanked by four Fe^{III} ions (Fe1, Fe2 and their symmetry partners) (Fig. 2c,d). In contrast to **1** where four Ce^{IV} ions form a central cubane-like $\{Ce_4(\mu_3\text{-}O)_4\}$ core, in **2**, Ce^{IV} ions are organized in a rhombus-shaped $\{Ce_4(\mu_4\text{-}O)_2(\mu_3\text{-}O)_2\}$ core. Here, metal ions are precisely coplanar with two oxygen atoms of the μ_4-O and μ_3-O ligands that are located on each side of the rhombus-shaped Ce_4 plane. The μ_4-O (O1 and its symmetry partner) and μ_3-O (O2 and its symmetry partner) deviate from this plane by 0.913 Å and 1.329 Å, respectively, thus having a flattened pyramidal arrangement of bonds. In the Ce_4 rhombus the side Ce···Ce separations are in the range of 3.7518(3)–3.7815(3) Å (Table 2) and the longest diagonal Ce···Ce distance is 6.526(5) Å. The interior Ce2–Ce1–Ce2($-x+1, -y, -z$) and Ce1–Ce2–Ce1($-x+1, -y, -z$) angles equal to 59.945(6)° and 120.06(1)°, respectively (Table S1). The flanked Fe ions are also organized in a rhombus shape with side Fe···Fe distances of 5.3289(6) and 5.448(1) Å, and the interior angles of 72.79(1) and 107.21(1)°, thus, such arrangement of metal ions in **2** can be viewed as a "Fe_4-rhombus-crossing-Ce_4-rhombus" (Fig. 3b). The dihedral angle between the rhombus-shaped Fe_4 and Ce_4 planes is 77.78°. An interesting feature of the molecular structure of **2** is that the $\{Fe_4Ce_4O_4\}$ core can also be conveniently described as two heterometallic $\{Fe_2Ce_2(\mu_3\text{-}O)_2\}$ butterfly subunits linked by one μ_3-O ion (O1 and its symmetry partner) in each unit that converts to a μ_4 mode, thus providing inter-butterfly bridge as shown in Fig. 3c. The metal topology in **2** is related to the "linked-butterfly" structure present in a homometallic mixed-valent octanuclear $(NBu^n_4)_2[Mn_8O_4(O_2CPh)_{12}(Et_2mal)_2(H_2O)_2]$ cluster reported by Christou et al. [42].

In cluster **2**, the coordinated MeOH forms a strong intramolecular O15–H15···O2 hydrogen bond of 2.627(4) Å with the μ_3-O atom, while the oxygen atom (O16) of solvent MeOH participates in the formation of the intermolecular O–H···O hydrogen bond of 2.815(7) Å with an oxygen atom of the chelating pivalate (Table S2). The crystal packing of **2** is shown in Fig. S4 (Supplementary Information).

In principle Fe^{III} entities can be both low ($S = 1/2$) and a high spin ($S = 5/2$). However, low spin complexes require strong ligands, normally π-acids, and a typical low spin Fe^{III} ion is $[Fe(CN)_6]^{3-}$. As there are no strong ligands present (including azide) in **1** and **2**, there is no reason to suspect a low spin Fe^{III} state. The Fe–N and Fe–O bond lengths observed are consistent with a high spin state [43].

Moreover, a search of the CSD indicates that for a $Fe^{III}N_6$ core, for which both high and low spin states are known, two maxima are found, one fairly distinct at 1.98 Å (consistent with low-spin) and one broad at 2.04–2.13 Å (consistent with high-spin), see Fig. S9 (bottom). As the covalent radius of oxygen is slightly smaller than for nitrogen by around 0.05 Å, one would expect a corresponding search for the $Fe^{III}O_6$ core to give maxima around 1.93 Å and 1.99–2.08 Å. What is found, see Fig. S9 (top), is one distinct maxima at 2.01 Å (around 1000 structures) and a very small peak at 1.94 Å (less than 20 structures), thus it seems low spin $Fe^{III}O_6$ cores are very rare. Again, the Fe–O and Fe–N bond lengths in **1** and **2** are consistent with a high spin state.

4. Conclusion

In conclusion, we adopted our synthetic approach to the preparation of two new heterometallic Fe^{III}-Ce^{IV} clusters **1** and **2** employing structure-directing amino alcohols and carboxylate bridges. Moreover, the use of μ_3-oxo trinuclear or μ_3-oxo hexanuclear pivalate species as precursors under the same synthetic conditions has a dramatic effect on the resulting metal topology in these clusters. The prepared octanuclear clusters **1** and **2** possess unprecedented close $\{Fe_4Ce_4(\mu_4\text{-}O)_4\}$ and open $\{Fe_4Ce_4(\mu_4\text{-}O)_2(\mu_3\text{-}O)_2\}$ cores. We are currently working on the diversification of this synthetic method by applying other amino alcohol ligands in Fe-Ce syntheses.

Declaration of Competing Interest

The authors declare that they have no known competing financial interests or personal relationships that could have appeared to influence the work reported in this paper.

Acknowledgments

S.G.B. thanks the Swedish Institute for financial support under the Visby Programme, F.M.A.N. and L.Ö. thank the Swedish Research Council. We thank Dr A. Ken Inge at Stockholm University and Dr. Christian Göb, Rigaku Europe SE, for assistance with the diffraction data collection.

Appendix A. Supplementary data

CIF files for the structures reported in this paper have been deposited with the Cambridge Crystallographic Data Centre (CCDC). The deposition numbers of clusters are CCDC 2019599 (**1**) and 2019600 (**2**). Copies of the data can be obtained, free of charge, on application to the CCDC, 12 Union Road, Cambridge CB21EZ, U.K. (fax 44 (1223) 336 033; e-mail deposit@ccdc.cam.ac.uk). Supplementary data to this article can be found online at https://doi.org/10.1016/j.ica.2020.120038.

References

[1] I.L. Malaestean, A. Ellern, S. Baca, P. Kögerler, Cerium oxide nanoclusters: commensurate with concepts of polyoxometalate chemistry? Chem. Commun. 48 (2012) 1499–1501.
[2] T. Montini, M. Melchionna, M. Monai, P. Fornasiero, Fundamentals and catalytic applications of CeO_2-based materials, Chem. Rev. 116 (2016) 5987–6041.
[3] J. Liu, L.R. Redfern, Y.J. Liao, T. Islamoglu, A. Atilgan, O.K. Farha, J.T. Hupp, Metal-organic-framework-supported and -isolated ceria clusters with mixed oxidation states, ACS Appl. Mater. Interfaces 11 (2019) 47822–47829.
[4] U. Bayer, D. Werner, C. Maichle-Mössmer, R. Anwander, Effective and reversible carbon dioxide insertion into cerium pyrazolates, Angew. Chem. Int. Ed. 59 (14) (2020) 5830–5836.
[5] Y.M. So, W.H. Leung, Recent advances in the coordination chemistry of cerium(IV) complexes, Coord. Chem. Rev. 340 (2017) 172–197.
[6] K. Liu, W. Shi, P. Cheng, Toward heterometallic single-molecule magnets: Synthetic strategy, structures and properties of 3d–4f discrete complexes, Coord. Chem. Rev. 289–290 (2015) 74–122.

[7] A. Mishra, A.J. Tasiopoulos, W. Wernsdorfer, E.E. Moushi, B. Moulton, M.J. Zaworotko, K.A. Abboud, G. Christou, Single-molecule magnets: a family of Mn^{III}/Ce^{IV} complexes with a $[Mn_8CeO_8]^{12+}$ core, Inorg. Chem. 47 (2008) 4832–4843.

[8] A. Baniodeh, Y. Lan, G. Novitchi, V. Mereacre, A. Sukhanov, M. Ferbinteanu, V. Voronkova, C.E. Anson, A.K. Powell, Magnetic anisotropy and exchange coupling in a family of isostructural $Fe^{III}_2Ln^{III}_2$ complexes, Dalton Trans. 42 (2013) 8926–8938.

[9] A. Draksharapu, W. Rasheed, J.E.M.N. Klein, L. Que Jr., Facile and reversible formation of Fe(III)–O–Ce(IV) adducts from nonheme oxoiron(IV) complexes and Ce(III), Angew. Chem., Int. Ed. 56 (2017) 9091–9095.

[10] C.M. Kizas, C. Papatriantafyllopoulou, M.J. Manos, A.J. Tasiopoulos, Heterometallic Fe^{III}–Ce^{IV} complexes from the use of aliphatic aminoalcohol ligands, Polyhedron 52 (2013) 346–354.

[11] J. Schläfer, S. Stucky, W. Tyrra, S. Mathur, Heterobi- and trimetallic cerium(IV) tert-butoxides with mono-, di-, and trivalent metals (M = K(I), Ge(II), Sn(II), Pb(II), Al(III), Fe(III)), Inorg. Chem. 52 (7) (2013) 4002–4010.

[12] V. Mereacre, D. Prodius, C. Turta, S. Shova, G. Filoti, J. Bartolomé, R. Clérac, C.E. Anson, A.K. Powell, The synthesis, structural characterization, magnetochemistry and Mössbauer spectroscopy of $[Fe_3LnO_2(CCl_3COO)_8H_2O(THF)_3]$ (Ln = Ce, Pr, Nd, Sm, Eu, Gd, Tb, Dy, Ho, Lu and Y), Polyhedron 28 (14) (2009) 3017–3025.

[13] Q.-F. Xie, Y.-M. Chen, M.-L. Huang, Bis[tris(1,10-phenanthroline)-iron(III)] tris(5,6-dioxybenzene-1,3-disulfonato)-cerium(III)-iron(III) hexahydrate, Wuji Huaxue Xuebao (Chin.) (Chin. J. Inorg. Chem.) 26 (2010) 263.

[14] H. Xue, Z. Zhang, R. Pan, B.-F. Yang, H.-S. Liu, G.-Y. Yang, Supramolecular nanotubes constructed from 3d–4f heterometallic sandwiched polyoxotungstate dimers, CrystEngComm 18 (2016) 4643–4650.

[15] M. Lammert, C. Glißmann, H. Reinsch, N. Stock, Synthesis and characterization of new Ce(IV)-MOFs exhibiting various framework topologies, Cryst. Growth Des. 17 (2017) 1125–1131.

[16] S. Waitschat, D. Fröhlich, H. Reinsch, H. Terraschke, K.A. Lomachenko, C. Lamberti, H. Kummer, T. Helling, M. Baumgartner, S. Henninger, N. Stock, Synthesis of M-UiO-66 (M = Zr, Ce or Hf) employing 2,5-pyridinedicarboxylic acid as a linker: defect chemistry, framework hydrophilisation and sorption properties, Dalton Trans. 47 (2018) 1062–1070.

[17] J.W. Sharples, D. Collison, The coordination chemistry and magnetism of some 3d–4f and 4f amino-polyalcohol compounds, Coord. Chem. Rev. 260 (2014) 1–20.

[18] L.R. Piquer, E.C. Sanudo, Heterometallic 3d–4f single-molecule magnets, Dalton Trans. 44 (2015) 8771–8780.

[19] S.G. Baca, J. van Leusen, M. Speldrich, P. Kögerler, Understanding the magnetism of $\{Fe_2Ln\}$ dimers, step-by-step, Inorg. Chem. Front. 3 (8) (2016) 1071–1075.

[20] I. Radu, V.C. Kravtsov, K. Krämer, S. Decurtins, S.-X. Liu, O.S. Reu, S.M. Ostrovsky, S.I. Klokishner, S.G. Baca, Synthesis, characterization and modeling of magnetic properties of a hexanuclear aminoalcohol-supported $Co^{II}_2Co^{III}_2Dy^{III}_2$ pivalate cluster, J. Phys. Chem. C 120 (2016) 7435–7443.

[21] O. Botezat, J. van Leusen, V.C. Kravtsov, P. Kögerler, S.G. Baca, Ultralarge 3d/4f coordination wheels: from carboxylate/amino alcohol-supported $\{Fe_4Ln_2\}$ to $\{Fe_{18}Ln_6\}$ rings, Inorg. Chem. 56 (2017) 1814–1822.

[22] I. Radu, V.C. Kravtsov, S.M. Ostrovsky, O.S. Reu, K. Krämer, S. Decurtins, S.-X. Liu, S.I. Klokishner, S.G. Baca, Tetranuclear $\{Co^{II}_2Co^{III}_2\}$, octanuclear $\{Co^{II}_4Co^{III}_4\}$, and hexanuclear $\{Co^{III}_3Dy^{III}_3\}$ pivalate clusters: synthesis, magnetic characterization and theoretical modeling, Inorg. Chem. 56 (2017) 2662–2676.

[23] O. Botezat, J. van Leusen, J. Hauser, S. Decurtins, S.-X. Liu, P. Kögerler, S.G. Baca, A spontaneous condensation sequence from a $\{Fe_6Dy_3\}$ wheel to a $\{Fe_7Dy_4\}$ globe, Cryst. Growth Des. 19 (2019) 2097–2103.

[24] O. Botezat, J. van Leusen, P. Kogerler, S.G. Baca, Ultrasound-assisted formation of $\{Fe_6Ln/Y_4\}$ wheel-shaped clusters and condensed $\{Fe_4Ln/Y_2\}$ aggregates, Eur. J. Inorg. Chem. 16 (2019) 2236–2244.

[25] M. Darii, V.C. Kravtsov, K. Krämer, J. Hauser, S. Decurtins, S.-X. Liu, M. Affronte, S.G. Baca, Aggregation of a giant bean-like $\{Mn_{26}Dy_6\}$ heterometallic oxo-hydroxo-carboxylate nanosized cluster from a hexanuclear $\{Mn_6\}$ precursor, Cryst. Growth Des. 20 (2020) 33–38.

[26] N.V. Gerbeleu, A.S. Batsanov, G.A. Timko, I.T. Struchkov, K.M. Indrichan, G.A. Popovich, Synthesis and structure of tri- and hexanuclear μ_3-oxopivalates of iron(III), Dokl. Akad. Nauk SSSR (Russ.) 293 (1987) 364–367.

[27] A.S. Batsanov, Y.T. Struchkov, G.A. Timko, Crystal structure of hexanuclear iron(III) pivalate, $Fe_6(\mu_3\text{-}O)_2(\mu\text{-}OH)_2(\mu\text{-}Me_3CCO_2)_{12}$, Koord. Khim. (Russ.) 142 (1988) 266–270.

[28] SAINT-Plus, Version 8.34, Bruker AXS Inc.: Madison, Wisconsin, USA, 2004.

[29] G.M. Sheldrick, SADABS, software for empirical absorption correction, version 2. 05. University of Göttingen, Germany, 2004.

[30] L. Krause, R. Hersbt-Irmer, G.M. Sheldrick, D. Stalke, Comparison of silver and molybdenum microfocus X-ray sources for single-crystal structure determination, J. Appl. Crystallogr. 48 (2015) 3–10.

[31] Crysalis RED Oxford Diffraction Ltd. Abingdon, Oxfordshire, UK, 2005.

[32] Crysalis CCD, Oxford Diffraction Ltd. Abingdon, Oxfordshire, UK, 2005.

[33] G.M. Sheldrick, Crystal structure refinement with SHELXL. Acta Crystallogr. C. 71 (2015) 3-8.

[34] L.J. Barbour, X-seed 4: Updates to a program for small-molecule supramolecular crystallography, J. Appl. Cryst. 53 (2020) 1–6.

[35] O. Botezat, J. van Leusen, V.Ch. Kravtsov, A. Ellern, P. Kogerler, S.G. Baca, Iron(III) carboxylate/aminoalcohol coordination cluster with propeller-shaped Fe_8 cores: approaching reasonable exchange energies, Dalton Trans. 44 (2015) 20753–20762.

[36] S.G. Baca, M. Speldrich, J. van Leusen, A. Ellern, P. Kögerler, Undecametallic and hexadecametallic ferric oxo–hydroxo/ethoxo pivalate clusters, Dalton Trans. 44 (2015) 7777–7780.

[37] S.G. Baca, M. Speldrich, A. Ellern, P. Kögerler, $\{Fe_6O_2\}$-based assembly of a tetradecanuclear iron nanocluster, Materials 4 (2011) 300–310.

[38] P.L. Roulhac, G.J. Palenik, Bond valence sums in coordination chemistry. The calculation of the oxidation state of cerium in complexes containing cerium bonded only to oxygen, Inorg. Chem. 42 (2003) 118–121.

[39] S.M. Kanowitz, G.J. Palenik, Bond valence sums in coordination chemistry using oxidation-state-independent R_0 values. A simple method for calculating the oxidation state of iron in Fe-O complexes, Inorg. Chem. 37 (1998) 2086–2088.

[40] W. Liu, H.H. Thorp, Bond valence sum analysis of metal-ligand bond lengths in metalloenzymes and model complexes. 2. Refined distances and other enzymes, Inorg. Chem. 32 (1993) 4102–4105.

[41] J. Friedrich, D. Schneider, L. Bock, C. Maichle-Mössmer, R. Anwander, Cerium(IV) neopentoxide complexes, Inorg. Chem. 56 (2017) 8114–8127.

[42] M.W. Wemple, H.-L. Tsai, S. Wang, J.P. Claude, W.E. Streib, J.C. Huffman, D.N. Hendrickson, G. Christou, Tetranuclear and octanuclear manganese carboxylate clusters: preparation and reactivity of $(NBu^n_4)[Mn_4O_2(O_2CPh)_9(H_2O)]$ and synthesis of $(NBu^n_4)_2[Mn_8O_4(O_2CPh)_{12}(Et_2mal)_2(H_2O)_2]$ with a "linked-butterfly" structure, Inorg. Chem. 35 (1996) 6437–6449.

[43] N.G. Spitsyna, M.A. Blagov, V.A. Lazarenko, L.V. Zorina, A.N. Vasiliev, V.B. Krapivin, R.D. Svetogorov, O.V. Maximova, S.V. Simonov, E.B. Yagubskiia, Spin-crossover behavior of neutral iron(III) complexes with salicylaldehyde thio-, seleno- and semicarbazone ligands: experiment and theoretical analysis, Dalton Trans. 48 (2019) 9328–9336.